Environment International 131 (2019) 104970

Contents lists available at ScienceDirect

Environment International

journal homepage: www.elsevier.com/locate/envint

Mitigation of bidirectional solute flux in forward osmosis via membrane surface coating of zwitterion functionalized carbon nanotubes

Shiqiang Zou[a,1], Ethan D. Smith[b,1], Shihong Lin[c], Stephen M. Martin[b,*], Zhen He[a,*]

[a] Department of Civil and Environmental Engineering, Virginia Polytechnic Institute and State University, Blacksburg, VA 24061, USA
[b] Department of Chemical Engineering & Macromolecules Innovation Institute, Virginia Polytechnic Institute and State University, Blacksburg, VA 24061, USA
[c] Department of Civil and Environmental Engineering, Vanderbilt University, Nashville, TN 37235, USA

ARTICLE INFO

Handling Editor: Hefa Cheng

Keywords:
Forward osmosis
Reverse solute flux
Forward solute flux
Zwitterion
Membrane modification

ABSTRACT

Forward osmosis (FO) has emerged as a promising membrane technology to yield high-quality reusable water from various water sources. A key challenge to be solved is the bidirectional solute flux (BSF), including reverse solute flux (RSF) and forward solute flux (FSF). Herein, zwitterion functionalized carbon nanotubes (Z-CNTs) have been coated onto a commercial thin film composite (TFC) membrane, resulting in BSF mitigation via both electrostatic repulsion forces induced by zwitterionic functional groups and steric interactions with CNTs. At a coating density of 0.97 g m^{-2}, a significantly reduced specific RSF was observed for multiple draw solutes, including NaCl (55.5% reduction), $NH_4H_2PO_4$ (83.8%), $(NH_4)_2HPO_4$ (74.5%), NH_4Cl (70.8%), and NH_4HCO_3 (61.9%). When a synthetic wastewater was applied as the feed to investigate membrane rejection, FSF was notably reduced by using the coated membrane with fewer pollutants leaked to the draw solution, including NH_4^+-N (46.3% reduction), NO_2^--N (37.0%), NO_3^--N (30.3%), K^+ (56.1%), PO_4^{3-}-P (100%), and Mg^{2+} (100%). When fed with real wastewater, a consistent water flux was achieved during semi-continuous operation with enhanced fouling resistance. This study is among the earliest efforts to address BSF control via membrane modification, and the results will encourage further exploration of effective strategies to reduce BSF.

1. Introduction

Alternative water resources, e.g., via water reuse and desalination, are of significant interest for addressing mounting global water demand. Membrane-based treatment processes have been extensively developed to produce reusable water due to their reliable performance and compact footprint (Shannon et al., 2008). As an emerging membrane technology, forward osmosis (FO) is able to supply high-quality water by utilizing a natural osmotic pressure gradient, and can offer unique merits such as reduced pressure operation, low fouling propensity, excellent solute rejection, and relatively low energy consumption if proper regeneration/separation of draw solutes (DS) could be achieved (Zou et al., 2016). Advancement of FO-based technologies will need to address several technical bottlenecks, especially further enhancement of fouling resistance and mitigation of reverse solute flux (RSF). RSF is defined as the cross-membrane DS diffusion to the feed (She et al., 2012), and has thus far received less attention than enhancing fouling resistance in the FO field. RSF has been studied via mathematical modeling (Lu et al., 2014), and can be affected by factors such as intrinsic membrane parameters (e.g., thickness, tortuosity, and porosity) (McCutcheon and Elimelech, 2006) and solute characteristics (e.g., hydrated ion radius, aqueous diffusivity, solution viscosity, and ion charge) (Zhao and Zou, 2011). Gradual DS leakage via RSF can lead to reduced osmotic driven force, salinity buildup on the feed side, potential feed contamination, aggravated membrane fouling, and elevated operating costs due to the need to continuously replenish DS (Lu and He, 2015).

Increasing awareness of RSF's detrimental effects has led to the development of indirect and direct control strategies. Indirect RSF control focuses on addressing the consequence of RSF, i.e. salinity buildup on the feed side, and major approaches include solute removal by using microorganisms to eliminate/assimilate biodegradable DS (e.g., NH_4HCO_3) (Li et al., 2016) and integration of parallel desalination/separation process (e.g., microfiltration or electrodialysis) (Qiu et al., 2015; Zou and He, 2017a). Nonetheless, alleviation of salinity accumulation in the feed solution does not mitigate RSF itself. The leaching of DS via RSF still leads to economic loss in operation. Therefore, direct RSF control needs to be prioritized via smart DS

* Corresponding authors.
E-mail addresses: martinsm@vt.edu (S.M. Martin), zhenhe@vt.edu (Z. He).
[1] These authors contribute equally to this paper.

https://doi.org/10.1016/j.envint.2019.104970
Received 17 April 2019; Received in revised form 27 May 2019; Accepted 26 June 2019

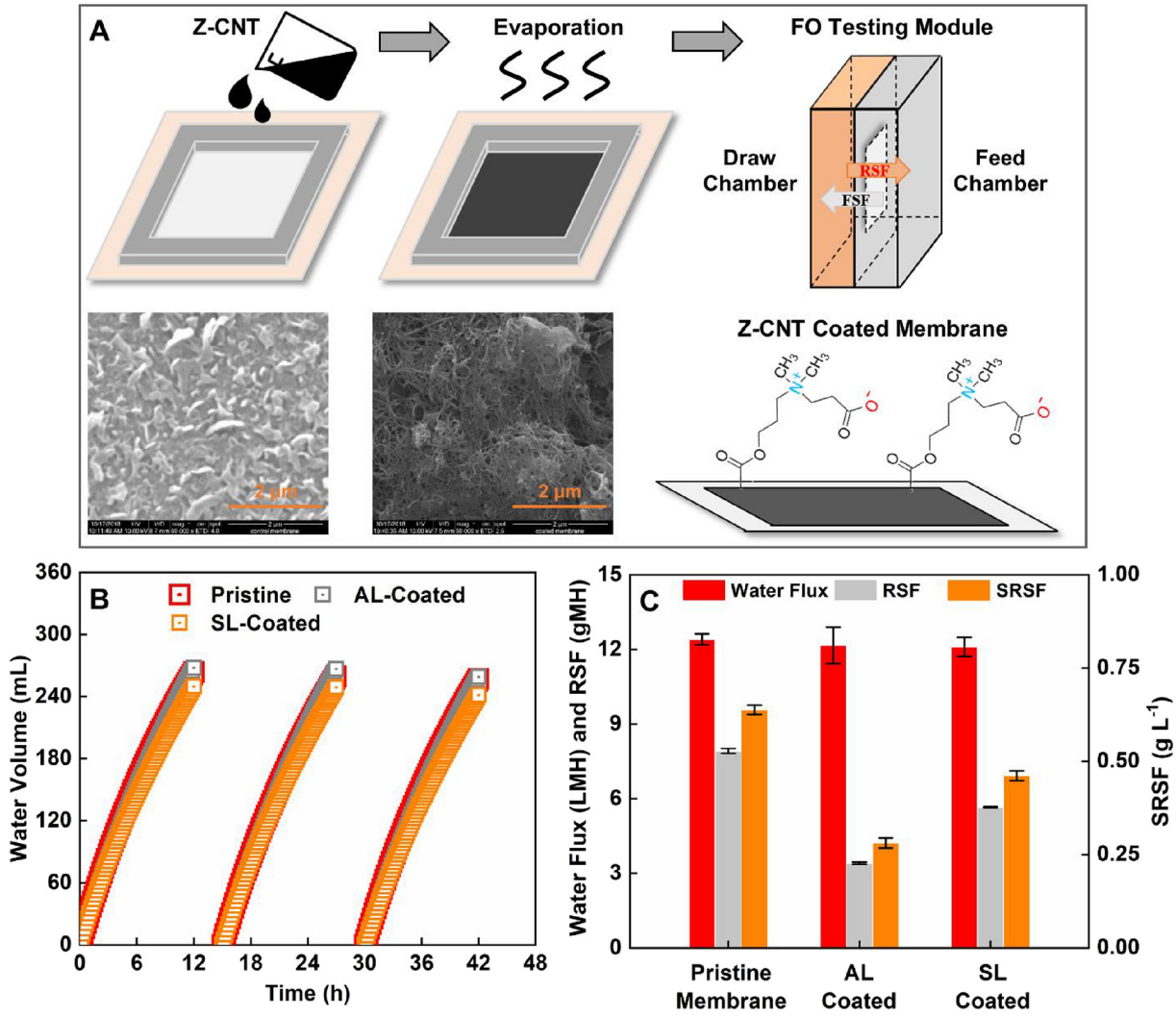

Fig. 1. (A) Schematic of the membrane coating and testing process, (B) comparison of water recovery volume among the pristine, AL-coated, or SL-coated membranes over three successive batch tests, and (C) quantification of the corresponding water flux, RSF and SRSF. In panel A, Z-CNT coating is confirmed by SEM image under 50,000 times magnification. In panels B and C, new pristine or coated membrane (0.97 g m^{-2}) was used for each batch test. In panel C, error bars represent triplicates with different membrane samples. Testing conditions: 100-mL 1-M NaCl as the draw and 500-mL DI water as the feed.

selection, operational strategies, and advanced membrane development (Zou et al., 2019). Novel DS, such as stimuli-responsive polymers, can theoretically produce low RSF, due to their large hydrodynamic diameter (> 100 nm), while achieving energy-efficient phase separation (Hartanto et al., 2015). Operational strategies have also been investigated, including pressure- (Blandin et al., 2013), electrolysis- (Zou and He, 2017b), and ultrasonic-assisted osmosis (Kowalski et al., 2015). However, additional energy is required to manipulate ion transport across the FO membrane, and inconsistent RSF reduction was reported due to potential membrane damage under a certain operating conditions (Lutchmiah et al., 2015).

Advanced membrane development aims at creating a better DS barrier via membrane fabrication or surface modification (Akther et al., 2015). New membrane fabrication techniques have yielded promising results in RSF reduction, including optimized substrate composition (Wang et al., 2015b), advanced substrate fabrication (Yasukawa et al., 2015), selection of novel supporting materials (Huang et al., 2013), and modified active layer composition (Kwon et al., 2015). Compared to membrane fabrication, surface modification via alterations of surface functional groups and hydrophilicity can be a straightforward method to enhance membrane performance (Guo et al., 2018). Zwitterionic monomers have emerged as an attractive surface modifier to enhance water flux and prevent adsorption of foulants in NF (Mi et al., 2017) and RO systems (Wang et al., 2015a), owing to their remarkable hydration capacity and electroneutrality (Zhou et al., 2014). Zwitterionic modification of FO membranes can lead to notable enhancement of fouling resistance (Wang et al., 2018), for example, a zwitterionic poly amino acid 3-(3,4-Dihydroxyphenyl)-$_L$-alanine ($_L$-DOPA) coated FO membrane exhibited up to 30% less fouling compared to an uncoated membrane (Nguyen et al., 2013). However, to the best of our knowledge, no prior studies have used zwitterionic materials for simultaneous RSF and forward solute flux (FSF) reduction (i.e. bidirectional flux reduction, BSF) in FO systems.

Herein, zwitterion functionalized carbon nanotubes (Z-CNT) have been coated onto a commercial Aquaporin Inside® FO membrane for performance enhancement (Holt et al., 2006) and BSF reduction. The specific objectives of this study are to (1) investigate the feasibility and consistency of RSF reduction by a Z-CNT coated FO membrane; (2) evaluate the effects of key operation parameters on RSF reduction, including Z-CNT coating density, DS concentration, and various DS species; (3) analyze membrane rejection (i.e., FSF) of the Z-CNT coated membrane; and (4) assess water flux consistency and membrane fouling resistance under semi-continuous operation.

2. Materials and methods

2.1. Z-CNT preparation, membrane coating, and characterization

The functionalization process and detailed characterization were conducted according to a previous study (Appendix A. Supplementary data) (Chan et al., 2016). The final zwitterion functional group attached to CNTs (25.2 wt%, equal to ~2 zwitterion groups per 100 carbon atoms, Supplementary data) had a positive charge at the tertiary amine group and a negative charge at the carboxylate group (Fig. S1, Supplementary data). Before membrane coating, a Z-CNT stock solution (1.0 mg mL^{-1}) was prepared by adding 20 mg Z-CNTs into 20 mL of deionized (DI) water, followed by probe sonication for 5 min (Fisher EB705 Probe Sonicator). After being cooled to room temperature, 10 mL of the Z-CNT solution (unless otherwise stated) was uniformly distributed onto the surface of a commercial TFC FO membrane (Aquaporin A/S, Denmark), which was placed under a Teflon frame and clamped onto a glass plate with either its active layer (i.e., AL-coated) or supportive layer facing up (i.e., SL-coated). Multiple batches of commercial membranes were coated (0.97 g CNT m^{-2}, unless otherwise stated) using the same protocol. The Z-CNT coated membranes were then placed inside a fume hood overnight to allow water to evaporate (Fig. 1A), and van der Waals force was expected to be the main binding force due to charged groups (e.g., hydroxyl and amine groups) between FO membrane surface and the functionalized Z-CNTs (Khalid et al., 2018; Park et al., 2016). The coated membrane was stored in DI water before use.

Both the pristine and coated FO membranes were characterized for zeta potential, membrane hydrophilicity, and surface morphology and composition. Membrane zeta potential was measured over a range of pH from 3.8 to 8.7 using a streaming potential analyzer (SurPASS, Anton Paar) with an adjustable gap cell and 1-mM KCl as the electrolyte. Hydrochloric acid (HCl) and potassium hydroxide (KOH) were used for pH adjustment. The membrane hydrophilicity was determined by measuring the contact angle (CA) of a sessile drop (DI water, ~25 μL) using an optical goniometer (KSV Instruments CAM 200). For each sample, at least three CA measurements were performed using different spots of the membrane surface. Membrane surface morphology was examined using field emission scanning electron microscopy (FESEM) with a 7-nm Pt/Pd coating (80:20 wt%, Leica ACE600 Sputter), with composition analysis performed using elemental mapping via energy dispersive spectroscopy (EDS).

2.2. Setup of FO testing cells

Two identical cross-flow FO testing cells were constructed, with one equipped with a pristine membrane (control system) and the other equipped with a coated membrane (AL-coated or SL-coated experimental system). Each solution chamber (5 × 5 × 1 cm) was connected to an external 600-mL reservoir. One piece of FO membrane (25 cm^2 effective area) was installed inside each testing module with its active layer facing the feed solution (i.e. AL-Feed, FO mode) to minimize potential membrane fouling. Upon membrane installation, the FO testing modules were rinsed with DI water at a flowrate of 120 mL min^{-1} for 3 h to remove unattached Z-CNT or other residue chemicals from the membrane surface. Under a default setting, 100-mL of 1-M NaCl (conductivity 86.8–87.1 mS cm^{-1}) and 500-mL of DI water were recirculated at a flowrate of 60 mL min^{-1} as the draw and feed solutions, respectively. The FO testing systems were operated under either a batch or a semi-continuous mode. During the batch operation (triplicate runs), both FO testing modules were operated for 12 h with water sampled at the beginning and the end of the experiment. Sufficient physical crossflow flushing (3 h with DI water, 60 mL min^{-1}) was performed between batch tests for membrane cleaning. During the semi-continuous operation, samples were taken daily with no membrane cleaning performed. All experiments were conducted in a temperature-controlled lab (20 ± 2 °C).

2.3. Experimental procedure

The Feasibility of RSF Reduction via Z-CNT surface coating was first investigated in three successive batch tests (under default settings) by comparing the performance between the pristine and coated membranes (AL-coated or SL-coated, 0.97 g m^{-2}). *The Effects of Operating Parameters* on FO performance (i.e. water flux and RSF) were then evaluated by using the AL-coated membranes with different Z-CNT coating densities (0, 0.10, 0.48, 0.97, or 1.45 g m^{-2}, equivalent to a stock solution volume of 0, 1, 5, 10, or 15 mL, respectively, Fig. S2), DS concentrations (0.25, 0.50, 0.75, or 1.00 mol L^{-1} NaCl), and DS compositions (0.25 mol L^{-1} NaCl, $(NH_4)_2HPO_4$, $NH_4H_2PO_4$, NH_4Cl, or NH_4HCO_3). Various coating densities were achieved by uniformly distributing 1, 5, 10, and 20 mL of the Z-CNT solution onto FO membrane surface. *Coating-Enhanced FSF Reduction* was subsequently analyzed using two different synthetic contaminated solutions as the feed (500 mL). The ions of significant interest include NH_4^+-N (111.5 ± 3.5 mg L^{-1}), NO_3^--N (110.1 ± 0.2 mg L^{-1}), NO_2^--N (119.6 ± 1.5 mg L^{-1}), K^+ (107.1 ± 1.4 mg L^{-1}), Mg^{2+} (100.1 ± 0.9 mg L^{-1}), and Ca^{2+} (99.8 ± 0.3 mg L^{-1}) in synthetic solution 1, or SO_4^{2-}-S (130.4 ± 2.2 mg L^{-1}) and PO_4^{3-}-P (131.8 ± 3.9 mg L^{-1}) in synthetic solution 2. This experiment design was to prevent potential precipitation within the synthetic solutions. Finally, *Water Flux Consistency* was explored with a focus on membrane fouling resistance via a 12-day semi-continuous operation, in which 100-mL 1-M NaCl (i.e. the draw) was replaced on a daily-basis, whereas the secondary effluent (500 mL constant, Table S1) from a local wastewater treatment plant (Christiansburg, VA) was supplied as the feed to achieve enhanced water reuse (Zou and He, 2016).

2.4. Measurement and analysis

Detailed water quality analysis is provided in Supplementary data. Quantification of water flux and RSF (J_s, gMH) was based on Eqs. (S1)–(S3) and (S4)–(S6), respectively (Zou and He, 2017a, 2017b). FSF (J_f, gMH) and membrane rejection (%) were determined to quantify the diffusion of feed solutes (FS, usually pollutants) to the draw solution (Eqs. (S7)–(S8)). Specific RSF (*SRSF*, g L^{-1}) was calculated to rule out the influence of both membrane structural parameters and bulk draw solution concentration (Phillip et al., 2010). *SRSF* quantifies the leakage of a DS or an ion that can leak across FO membrane to the feed side per unit of recovered water.

$$SRSF = \frac{J_s}{J_w} \tag{1}$$

RSF mitigation ratio (*MR*, %) was quantified by the ratio between the mitigated *SRSF* with coated membrane ($SRSF_m$) and that with the pristine membrane ($SRSF_o$).

$$MR = \left(1 - \frac{SRSF_m}{SRSF_o}\right) \times 100\% = \left(1 - \frac{J_{s,m}/J_{w,m}}{J_{s,o}/J_{w,o}}\right) \times 100\% \tag{2}$$

where $J_{s,o}$ and $J_{w,o}$ are the original RSF and water flux of the pristine membrane, respectively; $J_{s,m}$ and $J_{w,m}$ are the mitigated RSF and water flux of the coated FO membrane, respectively.

3. Results and discussion

3.1. RSF reduction via Z-CNT surface coating

The RSF reduction and water recovery capability of the Z-CNT coated membrane were investigated by comparing its performance to a pristine membrane. The FO system with the AL-coated membrane (0.97 g m^{-2}) could recover 264.5 ± 3.8 mL of water within 12 h,

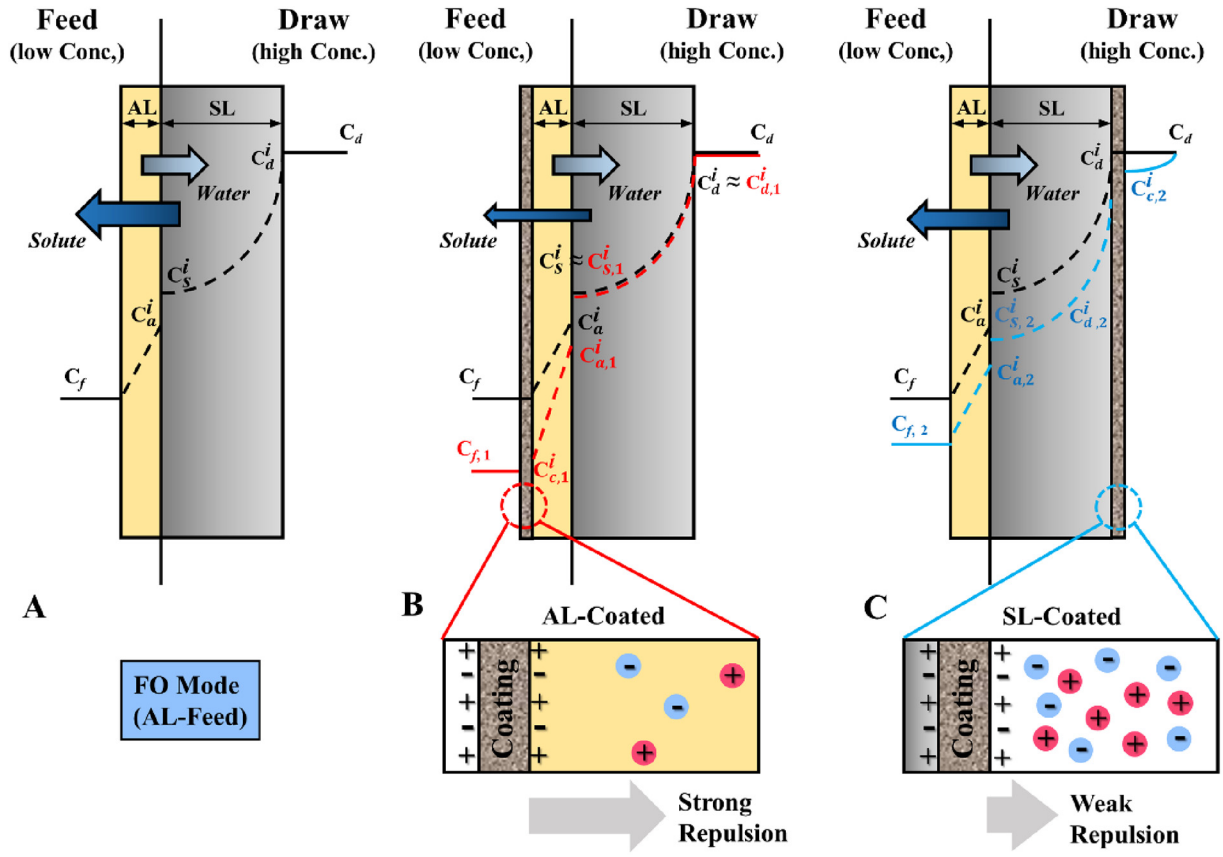

Fig. 2. The proposed DS ion diffusion pattern within (A) the pristine FO membrane; (B) the AL-coated membrane; and (C) the SL-coated membrane. The black line in each figure represents the original DS ion diffusion pattern, while the red and blue lines represent the DS ion diffusion affected by electrostatic repulsion induced by Z-CNT coating materials. Subscript 1 and 2 indicate DS diffusion pattern in AL-coated and SL-coated membranes, respectively. (For interpretation of the references to color in this figure legend, the reader is referred to the web version of this article.)

comparable to that of the pristine membrane (261.3 ± 2.2 mL, $p > 0.18$) but higher than that of the SL-coated membrane (246.6 ± 3.7 mL, $p < 0.05$, Fig. 1B). This result indicated that coating Z-CNTs on the dense and smooth active layer side had a negligible effect on water transport, whereas coating on the porous support layer resulted in a higher possibility of inner clogging, pore blockage, and a more severe internal concentration polarization, leading to reduced water extraction. It should be noted that the SL-coated membrane did exhibit a comparable maximum water flux (11.96 ± 0.94 LMH, Fig. 1C) to that of the pristine or AL-coated membranes (~12 LMH, $p > 0.46$), as this parameter was predominantly determined by the initial osmotic pressure gradient. In terms of RSF reduction, a notable decrease of both RSF and *SRSF* was observed with the coated membranes, compared to the pristine membrane (Fig. 1C), yielding an *MR* of 56.3% (AL-coated) and 28.1% (SL-coated), respectively.

The reduced RSF can be attributed primarily to the electrostatic repulsion force induced by the charged functional groups from the Z-CNTs on the membrane surface. For the pristine membrane, the diffusion of DS across the active layer (J_s^A) under the AL-Feed orientation (i.e. FO mode) can be described using Eq. (3) (Fig. 2A) (Phillip et al., 2010).

$$J_s^A = -D^A\frac{dC}{dt} = -\frac{D^A}{t_A}(C_a^i - C_f) = -\frac{D^A}{t_A}(C_a^i - 0) \quad (3)$$

where D^A is the diffusion coefficient of DS in active layer, t_A is the thickness of active layer, $C_a{}^i$ is the concentration of DS on the active layer side of the supportive layer-active layer interface, and C_f is the concentration of draw solute in the feed (assuming $C_f^i \approx C_f$ in an FO system with negligible external concentration polarization) (Cath et al., 2006). Initially, C_f is zero (DI water as the feed). Once the membrane surface is coated with Z-CNT, the negatively and positively charged functional groups provide an electrostatic repulsion against anions and cations that attempt to diffuse across the coating layer, resulting in a decrease in RSF ($J_{s,1}{}^A < J_s{}^A$ and $J_{s,2}{}^A < J_s{}^A$, where subscripts 1 and 2 represent the AL- and SL-coated orientations, respectively). To accurately measure the extent of net electrostatic repulsion, the Debye length (κ^{-1}, nm) is introduced (Eq. (4), for a symmetric monovalent electrolyte) (Russel et al., 1991). With decreasing Debye length, charges are increasingly electrically screened, providing reduced electrostatic repulsion force.

$$\kappa^{-1} = \sqrt{\frac{\varepsilon_r\varepsilon_0 RT}{2\times 10^3 F^2 C_0}} \quad (4)$$

where ε_0 is the permittivity of free space, ε_r is the dielectric constant, R is the gas constant, T is the temperature, F is the Faraday constant, and C_0 is the electrolyte concentration in molar units. Eq. (4) can be simplified as the following equation in the water solution at room temperature (~25 °C) (Israelachvili, 2011).

$$\kappa^{-1}(\text{nm}) = \frac{0.304}{\sqrt{I\,(\text{M})}} \quad (5)$$

where I is the ionic strength (molar unit) in the surrounding environment. This simplified Eq. (5) can further explain the *SRSF* reduction difference between the two coating orientations (i.e. $J_{s,1}{}^A < J_{s,2}{}^A$). Once coated on the active layer, Z-CNTs are exposed to a less concentrated environment with a relatively low ionic strength, due to the dilution effect of the clean water flux as well as rejection by the active layer ($C_{c,1}{}^i \ll C_d$, $C_{c,1}{}^i$ represents DS concentration at the interface of the coating layer for an AL-coated membrane). Thus, a relatively large

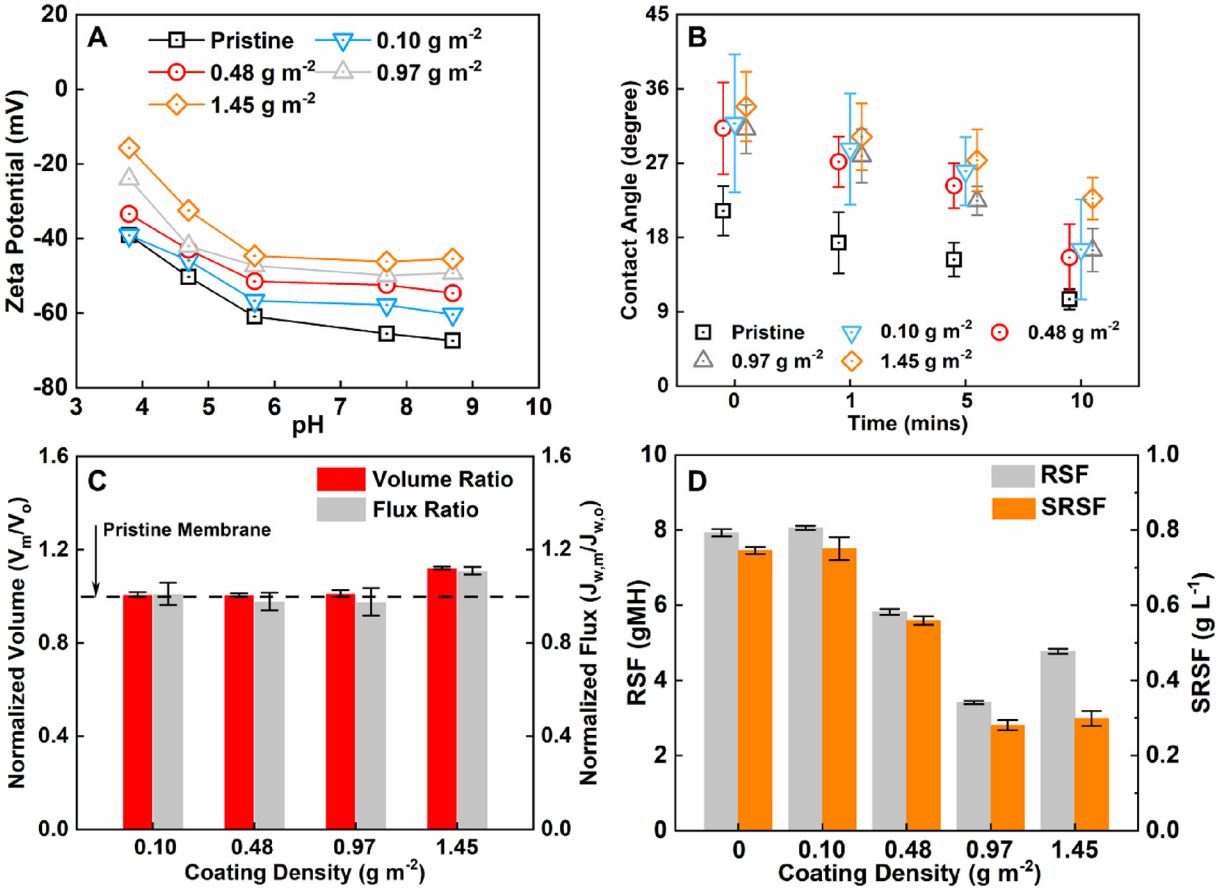

Fig. 3. Comparison of FO performance and membrane characterization among various coating densities regarding (A) membrane zeta potential; (B) membrane contact angle; (C) normalized water recover volume and maximum water flux to that of the pristine membrane; and (D) RSF and SRSF values. Membrane coating densities include 0 (pristine membrane), 0.48, 0.97, and 1.45 g m^{-2}. In panels C and D, triplicate tests were performed for coated membrane at each coating density. Error bars were calculated from triplicate test results by using the same membrane sample under each coating density. Testing conditions: 100-mL 1-M NaCl as the draw and 500-mL DI water as the feed.

Debye length and an extensive electrostatic repulsion leads to enhanced RSF reduction (Fig. 2B). Coating on the supportive layer, nonetheless, allows Z-CNTs to be directly exposed to the highly concentrated draw solution ($C_{c,2}{}^{i} \approx C_d$, $C_{c,2}{}^{i}$ represents the DS concentration at the interface of the coating layer in a SL-coated membrane), resulting in a smaller Debye length, a weakened electrostatic repulsion force due to the strong screening effect, and a smaller reduction in RSF (Fig. 2C). Considering the overall system performance, the AL-coated membrane was chosen for subsequent experiments.

3.2. Effects of Z-CNT coating density

Surface coating density (0, 0.10, 0.48, 0.97, and 1.45 g m^{-2}), as a key operating parameter, was investigated to assess its effects on zeta potential, membrane hydrophilicity, water flux, and RSF. In terms of zeta potential, the pristine FO membrane exhibited a negative charge due to abundant carboxylic groups (-COOH) on the TFC membrane (Fig. 3A) (Tiraferri and Elimelech, 2012). A more negatively charged surface (from −39.1 to −67.4 mV) was observed with higher pH due to stronger deprotonation of the carboxylic groups (Jin et al., 2012). Surface charge neutralization was observed with Z-CNT coating, consistent with the results of a prior zwitterionic coating study (Wang et al., 2018). With an increase of coating density, the zeta potential became less negative. For example, at a pH of 5.7, the surface charge increased from −60.9 mV (pristine membrane) to −46.2 mV (1.45 g m^{-2}). Such a positive shift towards neutral surface charge could hinder Donnan-facilitated cation transport (Sarkar et al., 2010) while minimizing the diffusion of counter anions to maintain solution electroneutrality (Epsztein et al., 2018). For membrane hydrophilicity, the dominance of the hydrophobic CNT backbone (74.8 wt%) over the hydrophilic zwitterionic functional groups (25.2 wt%) resulted in higher contact angles compared to that of the pristine membrane, even at a low coating density of 0.10 g m^{-2} (Fig. 3B) (Tijing et al., 2016; Wang et al., 2018). Increasing the coating density did not significantly affect membrane hydrophilicity, and the largest contact angle was observed under 1.45 g m^{-2} (an average of 28.5 ± 4.1°).

The effect of coating density on water recovery was subsequently investigated by using DI water as the feed (Fig. 3C). At lower coating densities (0.10–0.97 g m^{-2}), the volumes of recovered water (~247 mL) and water fluxes (10–13 LMH) were comparable to those of the pristine membrane. This could result from a dynamic balance between a negligible mass transport resistance added owing to the Z-CNT coating and enhanced water permeation via zwitterionic groups. A further density increase to 1.45 g m^{-2} yielded in an increased recovered water volume (293.2 ± 1.5 mL, $p < 0.01$) and water flux (13.8 ± 0.2 LMH, $p < 0.01$), suggesting that a higher density of surface zwitterionic groups could facilitate water transport. The performance of RSF reduction was closely linked to coating densities (Fig. 3D) and effective surface electrostatic repulsion force. A lower coating density provided limited surface electrostatic repulsion, rendering a comparable RSF. With a higher coating density, a gradual decrease in both RSF and *SRSF* was observed. The lowest RSF and *SRSF* were 3.41 ± 0.04 gMH and 0.281 ± 0.013 g L^{-1}, respectively, with a coating density of 0.97 g m^{-2}, resulting in an *MR* of 55.5% compared to

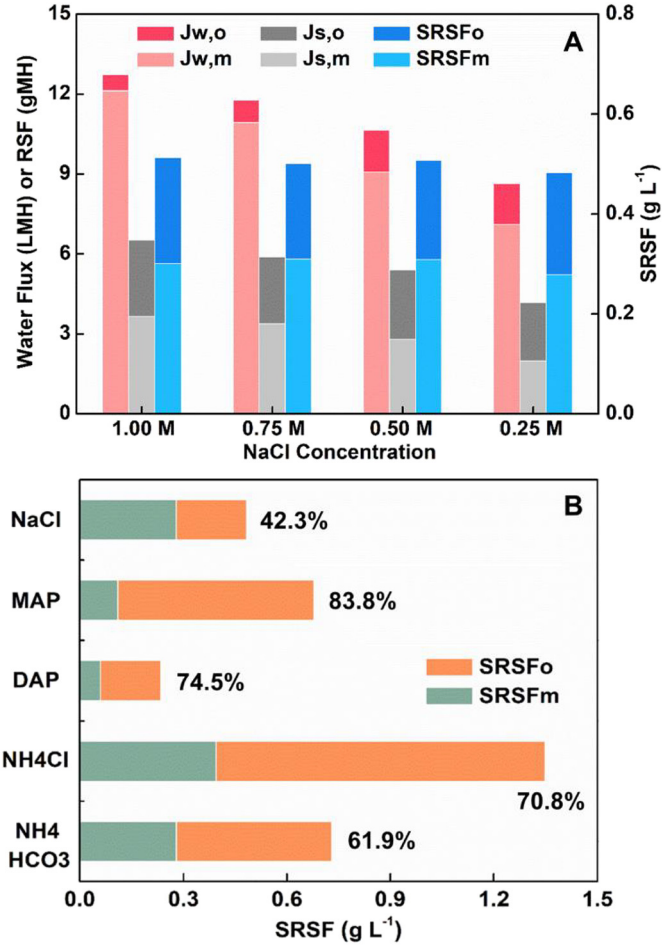

Fig. 4. Comparison of FO performance between pristine and coating-AL membranes in terms of (A) various draw solution concentration (NaCl) and (B) various draw solutes. The subscripts o and m in panel A represent pristine membrane and AL-coated membrane (0.97 g m^{-2}), respectively. In panel B, the concentration for all the draw solutions is 0.25 M, and the *MR* of each DS is labelled beside the column (i.e., $(1 - SRSF_m / SRSF_o) \times 100\%$).

that of the pristine membrane ($SRSF_o$ of 0.631 ± 0.008 g L^{-1}). A further increase of density to 1.45 g m^{-2} led to an increase in RSF (4.77 ± 0.07 gMH) due to a higher water recovery volume (Fig. 3C) and potentially diminished electrostatic repulsion via surface charge neutralization (Fig. 3A). However, a similar *SRSF* (0.299 ± 0.019 g L^{-1}, $p > 0.45$) was obtained to that of 0.97 g m^{-2} after normalizing RSF to water flux.

3.3. Effects of DS concentration and composition

To further investigate the relationship between ion concentration and the effectiveness of the electrostatic repulsion force (Eq. (5)), a series of DS concentrations (0.25, 0.50, 0.75, and 1.00 M NaCl) were tested as a key operating parameter. A gradual decrease in the draw concentration and osmotic driven force resulted in a reduced water flux for both the pristine ($J_{w,o}$) and the AL-coated membranes ($J_{w,m}$, Fig. 4A). Meanwhile, smaller amounts of NaCl leaked into the feed side with the lower draw concentration (0.25-M NaCl), leading to a RSF of 1.98 ± 0.10 gMH for the AL-coated ($J_{s,m}$) and 4.17 ± 0.16 gMH for the pristine membranes ($J_{s,o}$). A comparable *SRSF* was determined under 0.50–1.00 mol L^{-1} NaCl for the AL-coated membrane (0.301, 0.309, and 0.308 g L^{-1}, respectively), indicating a similar $C_{c,1}{}^{i}$ (DS level at the coating-active layer interface, Fig. 2B) and comparable Debye length (Eq. (5)). However, *SRSF* decreased to 0.279 ± 0.001 g L^{-1} ($SRSF_m$) when 0.25-M NaCl was tested with an AL-coated membrane. Hence, the Z-CNT coated FO membranes are more effective to electrostatically repel ions at lower DS concentrations (Eq. (5)). It is worth noting that a consistent *SRSF* was obtained for the pristine membrane under all DS concentrations (0.500 ± 0.011 g L^{-1}, $SRSF_o$), confirming that the *SRSF* of a certain DS in a selected pristine membrane was only affected by membrane intrinsic parameters (Phillip et al., 2010).

Various DSs were subsequently tested at 0.25 mol L^{-1} for *SRSF* reduction to evaluate the broad applicability of Z-CNTs. All the selected DSs were ammonium-based fertilizers and have been studied in fertilizer-driven FO (FDFO) to bypass energy-intensive DS regeneration/separation, including $NH_4H_2PO_4$ (monoammonium phosphate, MAP), $(NH_4)_2HPO_4$ (diammonium phosphate, DAP), NH_4Cl, and thermolytic NH_4HCO_3. Ammonium-based DSs were found to exhibit relatively large *SRSF* in commercial FO membranes (Achilli et al., 2010), compared to that of the benchmark NaCl (Fig. 4B). DAP, however, exhibited a much lower *SRSF* due to the higher mole amount of phosphate ions and their larger hydrated radii (Zou and He, 2017a). A significantly reduced *SRSF* was observed with the coated membrane (0.97 g m^{-2}) for all the DSs ($SRSF_m$, Fig. 4B), including MAP (0.110 ± 0.004 g L^{-1}, 83.8% *MR*), DAP (0.060 ± 0.002 g L^{-1}, 74.5% *MR*), NH_4Cl (0.394 ± 0.013 g L^{-1}, 70.8% *MR*), and NH_4HCO_3 (0.279 ± 0.009 g L^{-1}, 61.9% *MR*). The high degree of repulsion for multiple DS ions, especially nutrient ions (e.g., N and P) could effectively prevent contamination of the feed solution (e.g., brine water, groundwater, or wastewater) and reduce subsequent polishing costs before final discharge.

3.4. Membrane rejection and forward solute flux

FO has been recognized for its superior rejection of a variety of contaminants (over 95%) in the feed stream, such as inorganic pollutants (nutrients and heavy metals) (Xie et al., 2016), trace organic compounds (pharmaceuticals and pesticides) (Madsen et al., 2015), and microorganisms (Liu et al., 2013). However, minor permeation of exotic contaminants via FSF could lead to enhanced system costs for downstream processes (e.g., fouling and/or scaling during pressure- or thermal-separation) and potential environmental concerns if being directly reused (e.g., agriculture irrigation in FDFO). To quantify the magnitude of contaminant permeation via FSF, a synthetic solution containing common pollutant ions (each with a concentration of 100–130 mg L^{-1}) was fed into an FO cell equipped with the pristine membrane. The results indicated that multivalent ions (e.g., Mg^{2+} and $PO_4{}^{3-}$-P) exhibited significantly less permeation than monovalent ions ($NO_2{}^{-}$-N and K^+, Fig. 5A and Table S2), due to their relatively larger hydrated ion radii and better size exclusion effect. It should be noted that Ca^{2+} was completed rejected (i.e., 100% rejection rate) by the pristine membrane. Among the monovalent ions, cations ($NH_4{}^{+}$-N and K^+) demonstrated a higher propensity to diffuse towards the draw side than anions (NO^{2-}-N and NO^{3-}-N), owing to the negative membrane charge and Donnan facilitated cation transport (similar to RSF). $NH_4{}^{+}$-N had the lowest rejection rate (12.2 ± 1.2%) and the highest FSF (1.68 ± 0.02 gMH). Hence, membrane rejection must be properly addressed to promote water reuse.

Enhanced membrane rejection was realized by using the Z-CNT coated FO membrane. The AL-coated membrane (0.97 g m^{-2}) exhibited zero or negligible permeation of multivalent ions, with an FSF of 0 gMH (i.e., 100% rejection, Fig. 5A) for Mg^{2+}, Ca^{2+}, and $PO_4{}^{3-}$-P, and an FSF < 0.06 gMH for $SO_4{}^{2-}$-S (95.7 ± 0.2% rejection). Significantly improved rejection was also obtained for monovalent ions (Fig. 5A and B), including $NH_4{}^{+}$-N (49.8% rejection, FSF of 0.90 gMH, or 46.3% FSF reduction compared to pristine membrane), $NO_2{}^{-}$-N (83.6% rejection, FSF of 0.30 gMH, or 37.0% FSF reduction), $NO_3{}^{-}$-N (72.5% rejection, FSF of 0.54 gMH, or 30.3% FSF reduction), and K^+ (73.6% rejection, FSF of 0.43 gMH, or 56.1% FSF reduction). The enhanced rejection and reduced FSF could be attributed primarily to electrostatic repulsion as the Z-CNT was in direct contact with the feed. It should also be noted

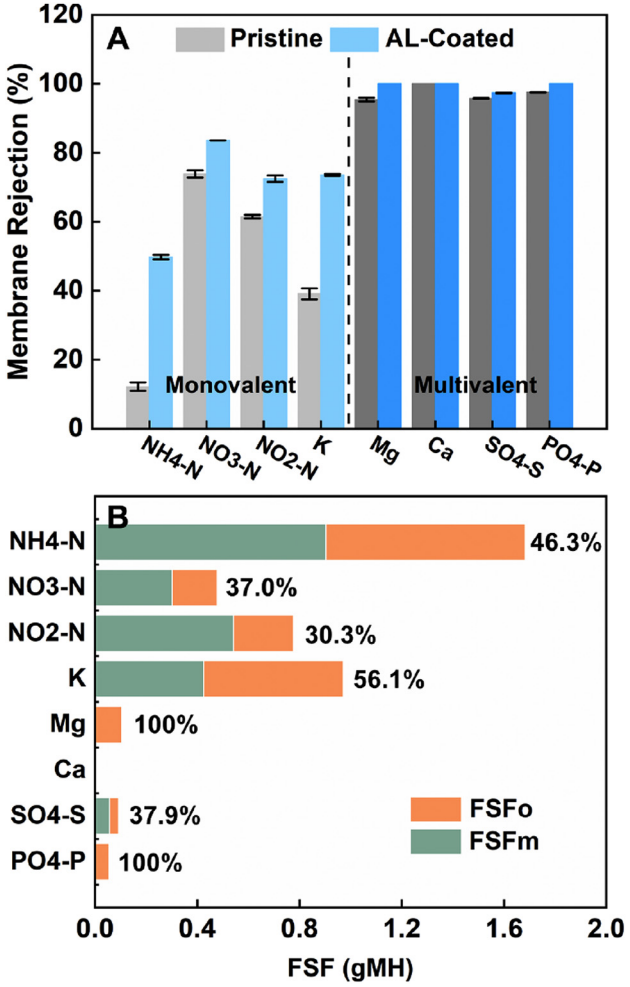

Fig. 5. Comparison of FO performance between pristine and AL-coated membranes in terms of (A) membrane rejection and (B) FSF of various pollutant ions in the feed. Synthetic solution, instead of DI water, was selected as the feed solution. The subscripts o and m in panel B legend represent pristine membrane and AL-coated membrane (0.97 g m^{-2}), respectively. The percentage represents for FSF reduction efficiency (i.e., $(1 - FSF_m / FSF_o) \times 100\%$). Error bars were calculated from triplicate test results with the pristine and AL-coated membranes.

that domestic wastewater tends to have lower ion concentrations (< 50 mg L^{-1}) than the synthetic solution used in this study (100–130 mg L^{-1}), resulting in elevated electrostatic repulsion forces based on Eq. (5). Together with a desirable RSF reduction, Z-CNT surface coatings have been proved to be effective in significantly decreasing BSF for multiple draw or feed solutes, allowing FO to potentially treat a variety of source waters (Lu et al., 2014).

3.5. Water flux consistency under semi-continuous operation

The lowest *SRSF* should be obtained by both minimizing DS penetration (i.e., low RSF) and more importantly, obtaining a consistent water flux under long-term operation (Eq. (1)). However, when fed with real wastewater, gradual fouling on the membrane surface could hinder efficient water transport through FO membrane while accelerating DS leakage via fouling-intensified concentration polarization (She et al., 2012). Zwitterionic materials, either coated on membrane surface or embedded inside the membrane, have been utilized to maintain water flux consistency in previous studies (Lee et al., 2018; Zhao et al., 2016). In this study, the Z-CNT coated FO membranes were further examined under semi-continuous operation focusing on water flux consistency and membrane fouling resistance (Fig. 6A). On day 1, less water (184.4 mL and 3.76 LMH) was recovered in the FO equipped with the AL-coated membrane compared to that of the pristine membrane (230.7 mL and 4.92 LMH). The reduced water extraction via coated membrane was likely due to the initial attraction of charged substances in the wastewater and potential accumulation of charged substances in the feed-membrane boundary layer, leading to additional water transport resistance and reduced water flux. As the operation continued, relatively consistent daily water recovery volumes and water fluxes were obtained with the coated membrane, while the pristine membrane exhibited a dramatic decrease. By the end of day 12, the AL-coated membrane exhibited only a 25.2% and 14.9% decrease in water volume and flux, respectively, much lower than the pristine membrane (50.4% and 54.5%, respectively). This desirable enhancement of fouling resistance is attributed to several possible mechanisms (He et al., 2016): (1) formation of a hydration shell assisted by zwitterionic materials on the membrane surface as a barrier to prevent direct contact of foulants (Chen et al., 2005); (2) steric hindrance effects induced by the chain of zwitterionic functional groups (Chen et al., 2010); and (3) potential antimicrobial properties of the CNT (Tiraferri et al., 2011), leading to an apparent visual difference of fouling coverage area on the membrane surface (Fig. 6B). Simple physical flushing appears to be very effective in removing most foulants on both membranes (day 13, Fig. 6B). On day 13 (after membrane cleaning), the recovery efficiency for the pristine membrane could reach 99.2%. However, flattened biofouling residues could still be observed under SEM (50 K magnification). For the AL-coated membrane, a higher than 100% recovery was observed after membrane cleaning due to detachment of Z-CNTs (Fig. 6B, SEM image after membrane cleaning). The elemental mapping via EDS indicated that the remaining foulants on the AL-coated membrane were marginally scattered inorganic scaling (e.g., Ca^{2+}, Fig. 6C), rather than biofouling.

3.6. Perspectives

Our results have collectively demonstrated effective control of bidirectional solute flux and consistent water flux by coating Z-CNTs on commercial FO membranes. To fully understand the contribution of each coating element to BSF reduction and antifouling performance, a direct membrane surface functionalization with zwitterionic groups and a pure CNT coating (without functionalization process) should be performed separately on commercial membranes and such a comparison may better reveal the underlying mechanisms. Several key challenges also need to be addressed to fully realize the potential of zwitterionic materials for the elimination of bidirectional solute flux. First, more robust approaches need to be employed to incorporate Z-CNTs onto the TFC membrane. Natural adhesion via physical adsorption in this study is one of the easiest, economically viable, and most scalable coating methods. However, Z-CNTs bond with FO active layer only through van der Waals force and may detach from the membrane during long-term operation (especially under higher hydraulic sheer force). The detached Z-CNTs can leave membrane surface together with accumulated foulants, rendering temporarily enhanced fouling resistance. Other strategies have been exploited in previous studies to strengthen the bond between zwitterionic materials and membrane surface, including grafting zwitterionic polymers via polymerization, surface segregation, and biomimetic adhesion (He et al., 2016). However, most of these strategies were only assessed for their performance in anti-fouling resistance rather than BSF mitigation. Alternatively, embedding zwitterionic materials inside the TFC membrane can offer a more permanent solution for possible detachment (Chan et al., 2016). Nonetheless, such an approach requires high compatibility between the zwitterionic material and the intrinsic membrane framework to maintain membrane integrity. Second, other zwitterionic materials than Z-CNTs should be explored for potential control of bidirectional solute flux in FO. The current Z-CNTs do provide a good electrostatic repulsion force to repel

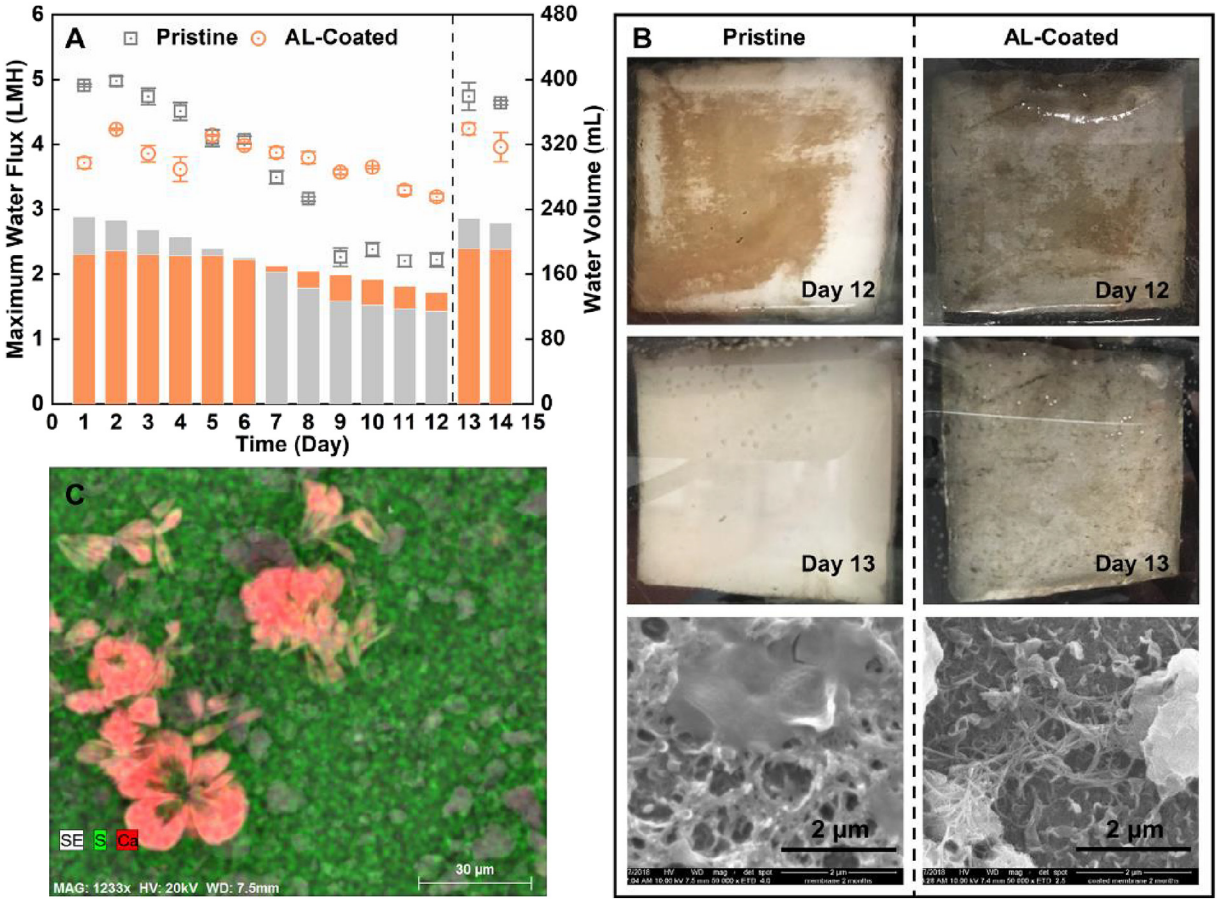

Fig. 6. Comparison of FO performance between pristine and AL-coated membranes under a semi-continuous operation in terms of (A) daily maximum water flux and recovery volume; (B) visual images of membrane on day 12 (before membrane cleaning) and day 13 (after membrane cleaning with SEM characterization); and (C) elemental mapping of AL-coated membrane (day 13) under EDS. In panel A, error bars were calculated by using the maximum water flux quantified at 20 min, 30 min, and 40 min of each cycle (23h). In panel C, the green and red color indicate sulfur from membrane framework and calcium from inorganic scaling. Raw secondary effluent from a local WWTP was collected as the feed solution. (For interpretation of the references to color in this figure legend, the reader is referred to the web version of this article.)

feed and draw solutes, yet it decreases the membrane hydrophilicity with larger surface contact angles. A hydrophilic polymer-based backbone, instead of a hydrophobic CNT, could be selected to carry the zwitterionic functional groups. Finally, in the case when zwitterionic materials (e.g., Z-CNT) detach from the membrane surface, their presence in the feed stream could lead to potential environmental concerns. The toxicity and ecological effects of such substances need to be comprehensively studied with further research.

4. Conclusions

In this study, zwitterion functionalized carbon nanotubes (Z-CNTs) have been coated onto a commercial thin film composite (TFC) membrane to achieve BSF mitigation via electrostatic repulsion forces induced by zwitterionic functional groups and steric interactions with CNTs. The results have important implications for promoting high-quality water recovery via FO and will inspire further development of effective strategies for BSF and fouling control. The following conclusions are reached:

- Better mitigation of RSF was achieved (under the AL-Feed mode) when coating Z-CNT on the active layer, rather than on the support layer, likely due to more extended electrostatic repulsion in the presence of lower ionic strength solutions.
- With an optimal coating density of 0.97 g m^{-2}, a significantly reduced specific RSF was observed for multiple draw solutes, including NaCl (55.5% reduction), $NH_4H_2PO_4$ (83.8%), $(NH_4)_2HPO_4$ (74.5%), NH_4Cl (70.8%), and NH_4HCO_3 (61.9%).
- FSF was notably reduced with fewer pollutants leaked to the draw solution, including NH_4^+-N (46.3% reduction), NO_2^--N (37.0%), NO_3^--N (30.3%), K^+ (56.1%), PO_4^{3-}-P (100%), and Mg^{2+} (100%). Successful BSF mitigation (both RSF and FSF) could allow FO to potentially treat a variety of source waters with a wide spectrum of DS.
- When fed with real wastewater, a much more stable water flux (only 14.9% decrease) was achieved with the Z-CNT coated membrane during a 12-day semi-continuous operation, compared to that of the pristine membrane (54.5% flux decline). Nearly all membrane foulants could be removed via simple physical flushing, rendering a more robust and cost-effective FO operation.
- This study is among the earliest efforts to address BSF control via FO membrane modification, and the results warrants further effort to explore alternative zwitterionic materials while strengthening the bond between coating materials and membrane surface.

Declaration of Competing Interest

The authors declare that they have no known competing financial interests or personal relationships that could have appeared to influence the work reported in this paper.

Acknowledgements

This research was financially supported by Institute for Critical Technology and Applied Science, Virginia Tech. Shiqiang Zou was partially supported by a Fellowship from Water INTERface IGEP at Virginia Tech. We sincerely thank Mr. Li Wang (Vanderbilt University) for his help with the analysis of membrane zeta potential and Virginia Tech Open Access Subvention Fund for covering publication expense.

Appendix A. Supplementary data

The functionalization process and characterization of Z-CNT, schematic of Z-CNT chemical structure (Fig. S1), surface coating density (Fig. S2), composition of secondary effluent from local WWTP (Table S1), hydrated ion radii (Table S2), detailed water quality analysis methods, and calculation equations for water flux, RSF, and FSF are provided in Appendix A. Supplementary data. Supplementary data to this article can be found online at doi:https://doi.org/10.1016/j.envint.2019.104970.

References

Achilli, A., Cath, T.Y., Childress, A.E., 2010. Selection of inorganic-based draw solutions for forward osmosis applications. J. Membr. Sci. 364 (1), 233–241.
Akther, N., Sodiq, A., Giwa, A., Daer, S., Arafat, H.A., Hasan, S.W., 2015. Recent advancements in forward osmosis desalination: a review. Chem. Eng. J. 281, 502–522.
Blandin, G., Verliefde, A.R., Tang, C.Y., Childress, A.E., Le-Clech, P., 2013. Validation of assisted forward osmosis (AFO) process: impact of hydraulic pressure. J. Membr. Sci. 447, 1–11.
Cath, T.Y., Childress, A.E., Elimelech, M., 2006. Forward osmosis: principles, applications, and recent developments. J. Membr. Sci. 281 (1), 70–87.
Chan, W.-F., Marand, E., Martin, S.M., 2016. Novel zwitterion functionalized carbon nanotube nanocomposite membranes for improved RO performance and surface antibiofouling resistance. J. Membr. Sci. 509, 125–137.
Chen, S., Zheng, J., Li, L., Jiang, S., 2005. Strong resistance of phosphorylcholine self-assembled monolayers to protein adsorption: insights into nonfouling properties of zwitterionic materials. J. Am. Chem. Soc. 127 (41), 14473–14478.
Chen, S., Li, L., Zhao, C., Zheng, J., 2010. Surface hydration: principles and applications toward low-fouling/nonfouling biomaterials. Polymer 51 (23), 5283–5293.
Epsztein, R., Shaulsky, E., Dizge, N., Warsinger, D.M., Elimelech, M.J.E.S., Technology, 2018. Role of ionic charge density in Donnan exclusion of monovalent anions by nanofiltration. Environ. Sci. Technol. 52 (7), 4108–4116.
Guo, H., Yao, Z., Wang, J., Yang, Z., Ma, X., Tang, C.Y., 2018. Polydopamine coating on a thin film composite forward osmosis membrane for enhanced mass transport and antifouling performance. J. Membr. Sci. 551, 234–242.
Hartanto, Y., Yun, S., Jin, B., Dai, S., 2015. Functionalized thermo-responsive microgels for high performance forward osmosis desalination. Water Res. 70, 385–393.
He, M., Gao, K., Zhou, L., Jiao, Z., Wu, M., Cao, J., You, X., Cai, Z., Su, Y., Jiang, Z., 2016. Zwitterionic materials for antifouling membrane surface construction. Acta Biomater. 40, 142–152.
Holt, J.K., Park, H.G., Wang, Y., Stadermann, M., Artyukhin, A.B., Grigoropoulos, C.P., Noy, A., Bakajin, O., 2006. Fast mass transport through sub-2-nanometer carbon nanotubes. Science 312 (5776), 1034–1037.
Huang, L., Bui, N.-N., Meyering, M.T., Hamlin, T.J., McCutcheon, J.R., 2013. Novel hydrophilic nylon 6, 6 microfiltration membrane supported thin film composite membranes for engineered osmosis. J. Membr. Sci. 437, 141–149.
Israelachvili, J.N., 2011. Intermolecular and Surface Forces. Academic Press.
Jin, X., Shan, J., Wang, C., Wei, J., Tang, C.Y., 2012. Rejection of pharmaceuticals by forward osmosis membranes. J. Hazard. Mater. 227–228, 55–61.
Khalid, A., Abdel-Karim, A., Ali Atieh, M., Javed, S., McKay, G., 2018. PEG-CNTs nanocomposite PSU membranes for wastewater treatment by membrane bioreactor. Sep. Purif. Technol. 190, 165–176.
Kowalski, S.J., Szadzińska, J., Pawłowski, A., 2015. Ultrasonic-assisted osmotic dehydration of carrot followed by convective drying with continuous and intermittent heating. Dry. Technol. 33 (13), 1570–1580.
Kwon, S.-B., Lee, J.S., Kwon, S.J., Yun, S.-T., Lee, S., Lee, J.-H., 2015. Molecular layer-by-layer assembled forward osmosis membranes. J. Membr. Sci. 488, 111–120.
Lee, W., Goh, P., Lau, W., Ong, C., Ismail, A.J.S., Technology, P., 2018. Antifouling zwitterion embedded forward osmosis thin film composite membrane for highly concentrated oily wastewater treatment. Sep. Purif. Technol. https://doi.org/10.1016/j.seppur.2018.07.009.
Li, X., Sun, S., Badgley, B.D., He, Z., 2016. Long-term performance and microbial community characterization of an osmotic anammox system for removing reverse-fluxed ammonium. Bioresour. Technol. 211, 628–635.
Liu, X., Qi, S., Li, Y., Yang, L., Cao, B., Tang, C.Y., 2013. Synthesis and characterization of novel antibacterial silver nanocomposite nanofiltration and forward osmosis membranes based on layer-by-layer assembly. Water Res. 47 (9), 3081–3092.
Lu, Y., He, Z., 2015. Mitigation of salinity buildup and recovery of wasted salts in a hybrid osmotic membrane bioreactor–electrodialysis system. Environ. Sci. Technol. 49 (17), 10529–10535.
Lu, X., Boo, C., Ma, J., Elimelech, M., 2014. Bidirectional diffusion of ammonium and sodium cations in forward osmosis: role of membrane active layer surface chemistry and charge. Environ. Sci. Technol. 48 (24), 14369–14376.
Lutchmiah, K., Harmsen, D.J.H., Wols, B.A., Rietveld, L.C., Jianjun, Q., Cornelissen, E.R., 2015. Continuous and discontinuous pressure assisted osmosis (PAO). J. Membr. Sci. 476, 182–193.
Madsen, H.T., Bajraktari, N., Helix-Nielsen, C., Van der Bruggen, B., Søgaard, E.G., 2015. Use of biomimetic forward osmosis membrane for trace organics removal. J. Membr. Sci. 476, 469–474.
McCutcheon, J.R., Elimelech, M., 2006. Influence of concentrative and dilutive internal concentration polarization on flux behavior in forward osmosis. J. Membr. Sci. 284 (1), 237–247.
Mi, Y.-F., Zhao, F.-Y., Guo, Y.-S., Weng, X.-D., Ye, C.-C., An, Q.-F., 2017. Constructing zwitterionic surface of nanofiltration membrane for high flux and antifouling performance. J. Membr. Sci. 541, 29–38.
Nguyen, A., Azari, S., Zou, L., 2013. Coating zwitterionic amino acid l-DOPA to increase fouling resistance of forward osmosis membrane. Desalination 312, 82–87.
Park, C.H., Tocci, E., Fontananova, E., Bahattab, M.A., Aljlil, S.A., Drioli, E., 2016. Mixed matrix membranes containing functionalized multiwalled carbon nanotubes: mesoscale simulation and experimental approach for optimizing dispersion. J. Membr. Sci. 514, 195–209.
Phillip, W.A., Yong, J.S., Elimelech, M., 2010. Reverse draw solute permeation in forward osmosis: modeling and experiments. Environ. Sci. Technol. 44 (13), 5170–5176.
Qiu, G., Law, Y.-M., Das, S., Ting, Y.-P., 2015. Direct and complete phosphorus recovery from municipal wastewater using a hybrid microfiltration-forward osmosis membrane bioreactor process with seawater brine as draw solution. Environ. Sci. Technol. 49 (10), 6156–6163.
Russel, W.B., Russel, W., Saville, D.A., Schowalter, W.R., 1991. Colloidal Dispersions. Cambridge University Press.
Sarkar, S., SenGupta, A.K., Prakash, P., 2010. The Donnan membrane principle: opportunities for sustainable engineered processes and materials. Environ. Sci. Technol. 44 (4), 1161–1166.
Shannon, M.A., Bohn, P.W., Elimelech, M., Georgiadis, J.G., Marinas, B.J., Mayes, A.M., 2008. Science and technology for water purification in the coming decades. Nature 452 (7185), 301–311.
She, Q., Jin, X., Li, Q., Tang, C.Y., 2012. Relating reverse and forward solute diffusion to membrane fouling in osmotically driven membrane processes. Water Res. 46 (7), 2478–2486.
Tijing, L.D., Woo, Y.C., Shim, W.-G., He, T., Choi, J.-S., Kim, S.-H., Shon, H.K., 2016. Superhydrophobic nanofiber membrane containing carbon nanotubes for high-performance direct contact membrane distillation. J. Membr. Sci. 502, 158–170.
Tiraferri, A., Elimelech, M., 2012. Direct quantification of negatively charged functional groups on membrane surfaces. J. Membr. Sci. 389, 499–508.
Tiraferri, A., Vecitis, C.D., Elimelech, M., 2011. Covalent binding of single-walled carbon nanotubes to polyamide membranes for antimicrobial surface properties. ACS Appl. Mater. Interfaces 3 (8), 2869–2877.
Wang, J., Wang, Z., Wang, J., Wang, S., 2015a. Improving the water flux and bio-fouling resistance of reverse osmosis (RO) membrane through surface modification by zwitterionic polymer. J. Membr. Sci. 493, 188–199.
Wang, Y., Ou, R., Wang, H., Xu, T., 2015b. Graphene oxide modified graphitic carbon nitride as a modifier for thin film composite forward osmosis membrane. J. Membr. Sci. 475, 281–289.
Wang, J., Xiao, T., Bao, R., Li, T., Wang, Y., Li, D., Li, X., He, T., 2018. Zwitterionic surface modification of forward osmosis membranes using N-aminoethyl piperazine propane sulfonate for grey water treatment. Process. Saf. Environ. Prot. 116, 632–639.
Xie, M., Shon, H.K., Gray, S.R., Elimelech, M., 2016. Membrane-based processes for wastewater nutrient recovery: Technology, challenges, and future direction. Water Res. 89, 210–221.
Yasukawa, M., Mishima, S., Shibuya, M., Saeki, D., Takahashi, T., Miyoshi, T., Matsuyama, H., 2015. Preparation of a forward osmosis membrane using a highly porous polyketone microfiltration membrane as a novel support. J. Membr. Sci. 487, 51–59.
Zhao, S., Zou, L., 2011. Relating solution physicochemical properties to internal concentration polarization in forward osmosis. J. Membr. Sci. 379 (1), 459–467.
Zhao, D., Qiu, G., Li, X., Wan, C., Lu, K., Chung, T.-S., 2016. Zwitterions coated hollow fiber membranes with enhanced antifouling properties for osmotic power generation from municipal wastewater. Water Res. 104, 389–396.
Zhou, Q., Lei, X.-P., Li, J.-H., Yan, B.-F., Zhang, Q.-Q., 2014. Antifouling, adsorption and reversible flux properties of zwitterionic grafted PVDF membrane prepared via physisorbed free radical polymerization. Desalination 337, 6–15.
Zou, S., He, Z., 2016. Enhancing wastewater reuse by forward osmosis with self-diluted commercial fertilizers as draw solutes. Water Res. 99, 235–243.
Zou, S., He, Z., 2017a. Electrodialysis recovery of reverse-fluxed fertilizer draw solute during forward osmosis water treatment. Chem. Eng. J. 330, 550–558.
Zou, S., He, Z., 2017b. Electrolysis-assisted mitigation of reverse solute flux in a three-chamber forward osmosis system. Water Res. 115, 111–119.
Zou, S., Yuan, H., Childress, A., He, Z., 2016. Energy consumption by recirculation: a missing parameter when evaluating forward osmosis. Environ. Sci. Technol. 50 (13), 6827–6829.
Zou, S., Qin, M., He, Z., 2019. Tackle reverse solute flux in forward osmosis towards sustainable water recovery: reduction and perspectives. Water Res. 149, 362–374.